Zong-Tao Li
National and Local Joint Engineering Research Center of Semiconductor Display and Optical Communication Devices, South China University of Technology, Guangzhou 510641, China; Foshan Nationstar Optoelectronics Company, Ltd., Foshan 528000, China
e-mail: meztli@scut.edu.cn

Jia-Yong Liang
National and Local Joint Engineering Research Center of Semiconductor Display and Optical Communication Devices, South China University of Technology, Guangzhou 510641, China
e-mail: scut18719388200@163.com

Jia-Sheng Li[1]
National and Local Joint Engineering Research Center of Semiconductor Display and Optical Communication Devices, South China University of Technology, Guangzhou 510641, China; Foshan Nationstar Optoelectronics Company, Ltd., Foshan 528000, China
e-mail: jiasli@foxmail.com

Jie-Xin Li
National and Local Joint Engineering Research Center of Semiconductor Display and Optical Communication Devices, South China University of Technology, Guangzhou 510641, China
e-mail: jiexinli.jeson@foxmail.com

Yong Tang
National and Local Joint Engineering Research Center of Semiconductor Display and Optical Communication Devices, South China University of Technology, Guangzhou 510641, China
e-mail: ytang@scut.edu.cn

Scattering Nanoparticles-Induced Reflection Effect for Enhancing Optical Efficiency of Inverted Quantum Dots-Light-Emitting Diodes Combined With the Centrifugation Technique

Inverted packaging structure is a promising alternative for thermal isolation between light-emitting diode (LED) chips and quantum dot (QD) converters with effective heat dissipation. However, serious reflection loss occurs at the lead frame owing to the inverted bonding of LED chips. In this study, the scattering nanoparticles-induced reflection effect has been developed to enhance the optical efficiency of inverted QD-LEDs combined with the centrifugation technique. The strong back-scattered effect of boron nitride (BN) nanoparticles with a thin columnar structure is chosen for reflection enhancement according to the ray-tracing and finite different time-domain simulations. Furthermore, a centrifugation technique is introduced to control the equilibrium geometry of the BN-incorporating reflector (BNR) by changing the centrifugal speed. Results indicate that the luminous flux of inverted QD/BNR-LEDs using the optimized concave BNR structure largely increases by 82.8% compared with reference inverted QD-LEDs. The great enhancement is attributed to the light concentrated effect of the concave geometry and the strong diffusion reflection ability of BN scattering nanoparticles. Consequently, the smart design on reflection properties of inverted QD-LEDs is critical for achieving high optical performances. [DOI: 10.1115/1.4048034]

Keywords: light-emitting diode, quantum dot, inverted packaging, optical efficiency, boron nitride

1 Introduction

Light-emitting diodes (LEDs) are promising solid-state light sources with advantages such as high brightness, long lifetime, and compact size. [1] Since the commercialization of blue GaN-based LEDs [2], it becomes one of the most essential techniques to generate various color combining blue LEDs with color converters [3,4]. Generally, rare earth-based phosphor composites are as color converters and integrated with LED chips, which have been widely adopted in illumination and display systems [5]. Great efforts have targeted on optimizing the packaging structure of phosphor-converted LEDs (pcLEDs) to improve their luminous efficacy [6], operating temperature [7], and color quality [8], accelerating the practical applications of pcLEDs in our daily lives. Recently, quantum dots (QDs) attract great attention in LED packaging owing to their high photoluminescence quantum yield (PLQY), nanometer size, and narrow emission spectra [9–12]. It is reported that a wide color-gamut of ~120% NTSC can be obtained by replacing the conventional phosphor converters with QD converters [13]. In addition, QD-LEDs also become one of the most promising strategies to realize full color micro/mini devices to satisfy the future demands on high resolution display applications [10,14–17].

However, the optical efficiency of QD-LEDs is still—twice lower than that of pcLEDs [18] owing to the host matrix effect [19–23] and reabsorption loss of QDs [12,24]. The conversion efficiency of LEDs only using the QD converter is generally less than ~50%, indicating that over half of absorption energy is turned into heat in QD converters. Moreover, QDs are always dispersed in polymer matrix with low thermal conductivity, suppressing their heat dissipation [25–27]. Therefore, the low efficiency

[1]Corresponding author.

Contributed by the Electronic and Photonic Packaging Division of ASME for publication in the Journal of Electronic Packaging. Manuscript received February 2, 2020; final manuscript received July 27, 2020; published online August 27, 2020. Assoc. Editor: Xiaobing Luo.

leads to not only high energy consumption and low brightness, most importantly, but also a low optical stability caused by the naturally thermal instability of QDs [28]. Therefore, several strategies have been proposed to effectively increase the optical efficiency of QD-LEDs, including liquid packaging [19] and nanoparticles incorporating [12]. Specific to the QD-phosphor hybrid LEDs [29], the separation between QDs and phosphor is helpful to increase the efficiency by managing the interabsorption loss and back-scattered loss [30,31]. In addition, the LED chips are also great heat source once with watt-level injection power, leading to a fast degradation of QD converters within seconds [26]. In these situations, it is highly expected to remove the QD converter from LED chips for thermal isolation [27,32]. However, QDs are generally dispersed in polymer matrix with low thermal conductivity, and the naturally convection is insufficient for the heat dissipation of QDs. Our previous studies have proposed a metal-based inverted packaging structure to solve this problem [33], and the QD converter is still coated on the Al lead frame while the LED chip is removed to the top side. Here comes to a new challenge that all of blue light is extracted after undergoing reflection loss at the Al surface, leading to a low optical efficiency.

In this study, the scattering nanoparticles-induced reflection effect has been developed to enhance the optical efficiency of inverted QD-LEDs combined with the centrifugation technique. The ray-tracing and finite difference time-domain (FDTD) methods were conducted to investigate the scattering effect of nanoparticles on the reflection performance of inverted LEDs; accordingly, the boron nitride (BN) scattering nanoparticles with a thin columnar structure were selected. Then, a centrifugation technique was introduced to obtain BN-incorporating reflector (BNR) with different structures. The BN concentration and centrifugal speed were adjusted to successfully control the equilibrium geometry of BNR for achieving high efficiency devices.

2 Experiments

First, the BN composites were dispensed onto the Al lead frame to form a BNR. Then, the BNR-coated Al lead frame was fixed on a spin coater (EZ4 SPIN COATER, Jiangyin Jiatu Technology, Co., Ltd) with different centrifugal speed to adjust the curvature of the BNR, as shown in Figs. 1(*a*) and 1(*b*). After centrifugation, the Al lead frame was moved to the oven at a temperature of 90 °C for 1.5 h to cure the BNR. As for blue inverted BNR-LEDs, the indium tin oxide deposited glass (ITO glass) bonded with a blue LED chip was fixed on the top of the Al lead frame to establish the electrical connection between the LED chip and the lead frame. As for inverted QD/BNR-LEDs, QD composites were dispensed onto the BNR to form the QD converter before fixing the ITO glass, and the QD converter was cured at the same condition as the BNR. The diagram and photograph of inverted QD/BNR-LEDs are shown in Figs. 1(*c*) and 1(*d*), respectively. In our cases, the Al lead frame was selected considering the high thermal conductivity, and its size was 6.3 (length) × 6.3 (width) mm. The QD converter (PLQY of approximately 77%) is consisted with green CdSe-based QDs (PLQY of approximately 82%) and polydimethylsiloxane (PDMS) matrix; the QD concentration and the dispensing mass were kept at 1 wt.% and 5 mg (the thickness of a QD layer is approximately 80 μm), respectively. Its absorption and photoluminescence (PL) spectra are given in Fig. 2. The ITO glass was used for LED chip bonding, and the thickness of the glass and ITO layer is 1.1 mm and 185 nm, respectively. The LED chip is with a flip-chip structure with a size of 0.89 (length) × 0.89 (width) mm; the peak wavelength is 455 nm. The BNR was consisted with BN nanoparticles and PDMS matrix and the morphology of BN nanoparticles is given in Fig. 3, which were purchased from Aladdin reagent, Co., Ltd. The optical performances of devices were measured by an integrating system. All these tests were conducted under laboratory conditions with a constant ambient temperature of 22 °C.

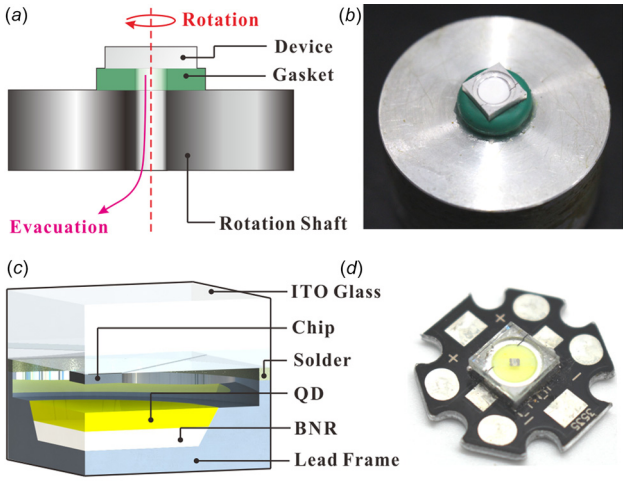

Fig. 1 (*a*) Diagram of centrifugal process of inverted LEDs. (*b*) Photograph of inverted BNR-LEDs fixed on the rotation shaft inserted with a gasket. (*c*) Cross-sectional diagram and (*d*) photograph of inverted QD/BNR-LEDs.

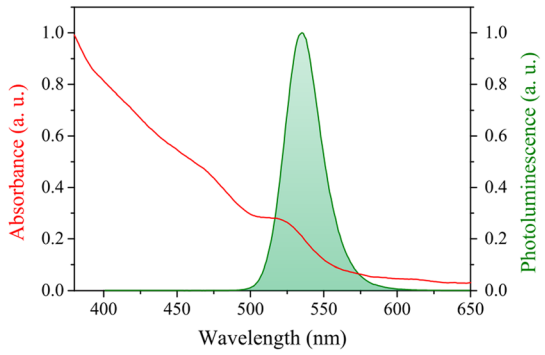

Fig. 2 The absorption and PL spectra of QD converter

3 Results and Discussion

3.1 Scattering Effect of Nanoparticles on Reflection Performance. Nanoparticles are generally used to reduce the total internal reflection loss and color deviation in conventional LED devices utilizing their scattering effect [34,35], while they are barely used for reflection enhancement. Therefore, a ray-tracing simulation is first conducted to investigate the scattering nanoparticles-induced reflection effect in order to provide some guidelines for designing BNR. To ensure the simulation accuracy,

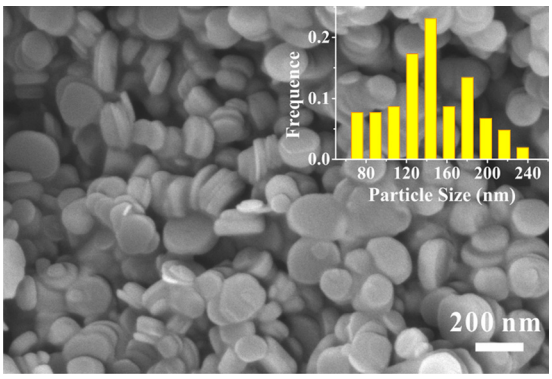

Fig. 3 The scanning electron microscope (SEM) images of BN nanoparticles. The insert shows the particle size distributions with an average size of 144 nm.

one million rays are used, and the threshold flux is 0.5%. In the Monte Carlo bulk scattering model, scattering coefficient and scattering distribution are used to determine the scattering phenomenon of nanoparticles in the matrix [36]. Herein, the Henyey–Greenstein function is used to represent the scattering distribution of nanoparticles, which is determined by the anisotropy coefficient g ranging from -1 to 1. A larger g indicates that much more incident light is front-scattered along the incident direction. The structural parameters are the same as the blue inverted LED device used in experiments, and the optical parameters are listed in Table 1; the color conversion processes are not considered for convenience. In addition, the thickness of the reflection layer is kept at 400 μm with an ideal planar structure. The absorption loss A is used to evaluate the optical efficiency of inverted LEDs in simulation, which is defined as follows:

$$A = P_{\text{abs}}/P_{\text{chip}} \tag{1}$$

where P_{abs} is the radiant power of blue light absorbed by Al lead frame; P_{chip} is the radiant power of LED chip without packaging. The absorption loss of inverted LEDs with different reflection layers is given in Fig. 4(*a*). The absorption loss is as high as 37.8% when the reflection layer is without scattering ability, demonstrating a serious optical loss of blue light. When the g is larger than -1, the absorption loss slightly increases as the scattering coefficient increases. This result can be attributed to the stronger front-scattered ability of the reflection layer that disturbs the propagation direction of incident blue light, increasing the total internal reflection at the interface between the reflection layer and the air. However, the absorption loss obviously reduces as the scattering coefficient keeps increasing owing to the increasing back-scattered ability, preventing the blue light from reaching at the Al lead frame. Although all the reflection layers contribute to an absorption loss smaller than 10% when the scattering coefficient is large enough ($\sim$650 mm^{-1}), it is not easy to achieve such a high scattering coefficient in practices considering the dispersity of nanoparticles. Fortunately, the reflection layer with a smaller g value can more easily obtain lower absorption loss at the same scattering coefficient. For example, the absorption loss is reduced from 25.7% to 9.4% as the g decreases from 0.75 to -1 at the same scattering coefficient of 100 mm^{-1}. These results are because that most blue light can escape from the reflection layer and then emit out from the ITO glass when nanoparticles have a strong back-scattered ability (small g values). While nanoparticles have a strong front-scattered ability (large g values) as shown in Fig. 4(*c*), most blue light can be absorbed by the lead frame. Therefore, the back-scattered ability of nanoparticles is essential to reduce the absorption loss by the Al lead frame.

Generally, the scattering distributions of the bulk layer are determined by the structure of their incorporated nanoparticles [37]. Therefore, a stronger back-scattered ability is highly expected for nanoparticles in the reflection layer. To provide a solid guidance to select nanoparticles for inverted LEDs with reflection enhancement, a FDTD simulation is conducted to investigate this issue. Herein, two typical nanoparticles with spherical and columnar geometry, respectively, are investigated in our cases, which are generally used in LED packaging. The three-dimensional FDTD model with total-field and scattered-field source is used to obtain the scattering behavior of nanoparticles, and the background refractive index is kept at 1.41, much more detailed can be found elsewhere [38]. To ensure the simulation accuracy, the minimum grid size located at the particle region is 2 nm, and the simulation time is set to be large enough (5000 fs) to ensure energy convergence. The scattering power distributions of spherical nanoparticles and columnar nanoparticles with different particle size d are given in Figs. 5(*a*) and 5(*b*), respectively. In this case, the columnar nanoparticles are with the thickness t as the same as their particle size, and the complex refractive index of all these nanoparticles is kept at 1.7 without absorption for incident light. All the light has an incident direction along 90 deg axis as shown in Fig. 5. It is assumed that the nanoparticles are randomly distributed in the reflection layer, which means that the probability of light propagating into these nanoparticles with different incident angles is the same. Therefore, the scattering power distributions of columnar nanoparticles are the average results considering three typical orienting angles of 0 deg, 45 deg, and 90 deg for simplification (the angles between the thickness direction and the light incident direction). As for spherical nanoparticles, all the orienting angles are the same owing to their structural symmetry. In Figs. 5(*a*) and 5(*b*), as the particle size decreases and becomes smaller than 100 nm, both of spherical nanoparticles and columnar nanoparticles appear a stronger back-scattered ability, which tends to be the Rayleigh scattering. However, the front-scattered ability also becomes stronger (wider front-scattered distribution) as the particle size decreases, which is not beneficial to achieve a higher back-scattered energy proportion. Nevertheless, nanoparticles with a smaller particle size (smaller than 100 nm) can be considered in the reflection layer owing to its more obvious back-scattered ability.

We also investigate the scattering power distributions of columnar nanoparticles with different thickness, as shown in Fig. 5(*c*), their complex refractive index is also set as 1.7, and their particle size is kept at 150 nm. It is interesting that the back-scattered power largely increases as the thickness decreases while the front-scattered power only slightly increases, which tends to be saturated at a thickness of 20 nm. These results demonstrate that nanoparticles with a thinner columnar geometry are more expected in the reflection layer in order to enhance the back-scattered energy proportion. To have a deeper understanding on this issue, the cross-sectional electromagnetic fields of nanoparticles with different orienting angles are given in Figs. 6(*a*) and 6(*b*), which are associated with the thickness of 150 and 20 nm, respectively. As shown in Fig. 6(*a*), most of the electromagnetic energy is concentrated at the front direction for thick columnar nanoparticles ($t = 150$ nm) with different orienting angles, and it is because that their feature size is almost the same at different direction. As for the thin columnar nanoparticles ($t = 20$ nm) shown in Fig. 6(*b*), electromagnetic power around them becomes stronger as the orienting angles increase. These results can be attributed to the smaller future size along the light incident direction when the light is perpendicularly incident into the end surface, leading to a weaker scattering intensity. Their corresponding scattering power distributions with the thickness of 150 and 20 nm are also given in Figs. 6(*c*) and 6(*d*), respectively. It is clear that the scattering power distributions are almost the same as thick columnar nanoparticles with different orienting angles, while they show great difference for thin columnar nanoparticles. It is interesting that the back-scattered energy proportion of thin columnar nanoparticle with 0 deg orienting angle is even comparable with its front-scattered energy proportion. As discussed in Fig. 6(*b*), this result can be attributed to the light incident along the thickness direction with the smallest feature size of 20 nm, which is more satisfied with the Rayleigh scattering with a high back-scattered energy

Table 1 Optical parameters used in ray-tracing simulation of inverted LEDs

Object	Reflectance (%)	Refractive index	Absorption coefficient (mm^{-1})
Al lead frame	60	—	—
ITO	85	—	—
n-GaN	—	2.43	0
MQW	—	2.43	5
p-GaN	—	2.43	0
Ag Reflector	98	—	—
Sapphire	—	1.84	0
Silicone	—	1.41	0

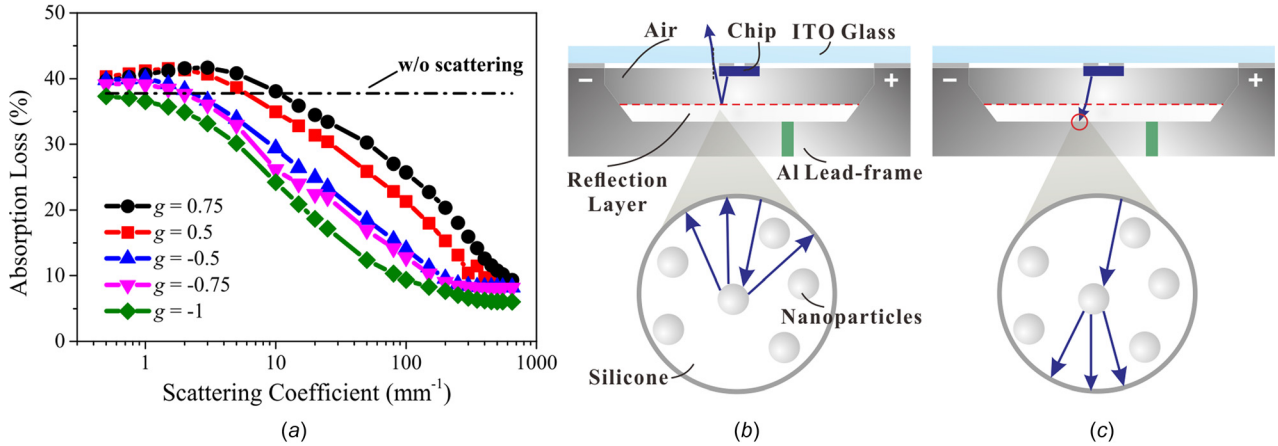

Fig. 4 Ray-tracing simulations of inverted LEDs with different reflection layers. (*a*) Absorption loss of inverted LEDs using reflection layers with various scattering coefficient and anisotropy coefficient *g*. ((*b*) and (*c*)) Diagrams of light-extraction mechanisms of inverted LEDs using reflection layers with strong back-scattered ability (small *g* values) and front-scattered ability (large *g* values), respectively.

proportion. Therefore, the Rayleigh scattering along the thickness direction with small size is the major factor that results into a strong back-scattered ability for thin columnar nanoparticles. In future, it is great potential to further increase the back-scattered ability by carefully orienting the thin columnar nanoparticles to ensure the light perpendicularly incident into the end surface. In addition, a higher refractive index is also beneficial to increase the back-scattered ability of these thin columnar nanoparticles ($t = 20$ nm) as shown in Fig. 5(*d*), which can be originated from the stronger diffraction effect.

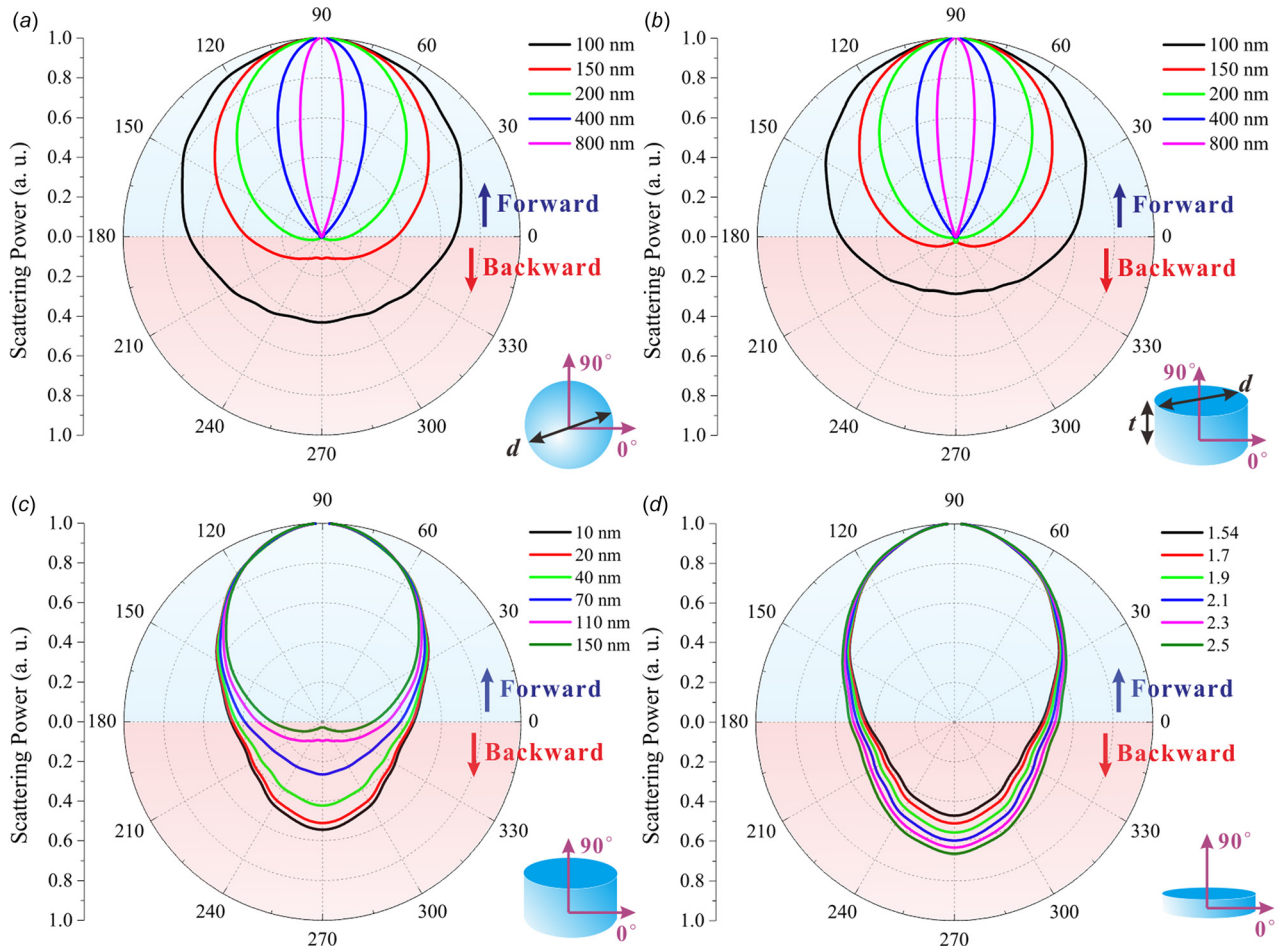

Fig. 5 Scattering power distributions of nanoparticles. ((*a*) and (*b*)) Spherical and columnar nanoparticles with different particle sizes *d*, respectively; the thickness *t* of columnar nanoparticles is equal to particle size *d* in these cases. (*c*) Columnar nanoparticles with different thicknesses *t*; the particle size *d* is kept at 150 nm. (*d*) Columnar nanoparticles with different refractive index; the particle size *d* and thickness *t* are kept at 150 and 20 nm, respectively. All the scattering power distributions of columnar nanoparticles are the average results obtained by source with 0 deg, 45 deg, and 90 deg incident angles.

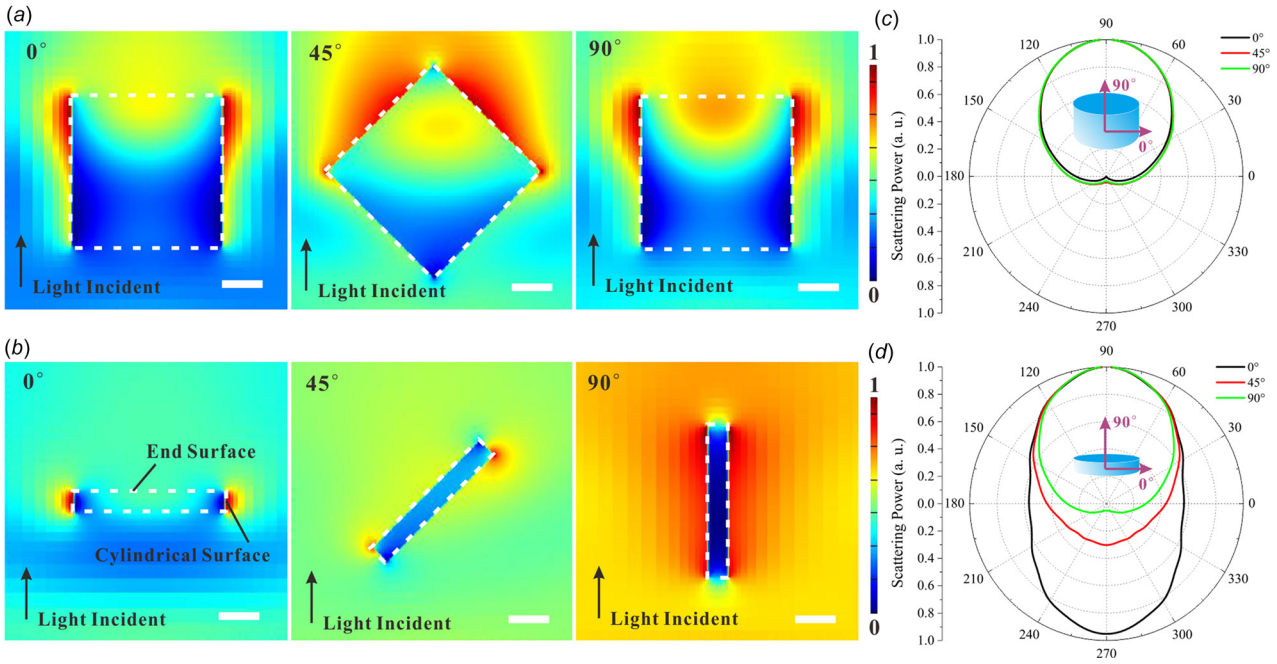

Fig. 6 ((*a*) and (*b*)) Cross-sectional electromagnetic fields and ((*c*) and (*d*)) scattering power distributions of columnar nanoparticles with different orienting angles. ((*a*) and (*c*)) Thick columnar nanoparticles ($t = 150$ nm). ((*b*) and (*d*)) Thin columnar nanoparticles ($t = 20$ nm). ((*a*) and (*b*)) The unit of column bar is a. u., and the scale bar is 40 nm. The columnar nanoparticle is located within the dotted line.

3.2 Effect of Boron Nitride-Incorporating Reflector Structure on Chip Light Extraction. According to above theoretical analysis on the back-scattered ability of nanoparticles, BN nanoparticles with a thin columnar structure (average particle size of 144 nm and thickness of 26 nm as shown in Fig. 3) are selected as scattered centers in the reflection layer. In addition, a higher concentration is expected to achieve a larger scattering coefficient, which is beneficial to obtain a stronger reflection performance as discussed above. The reflection spectra of BNR with different BN concentrations are given in Fig. 7(*a*), and the membrane thickness

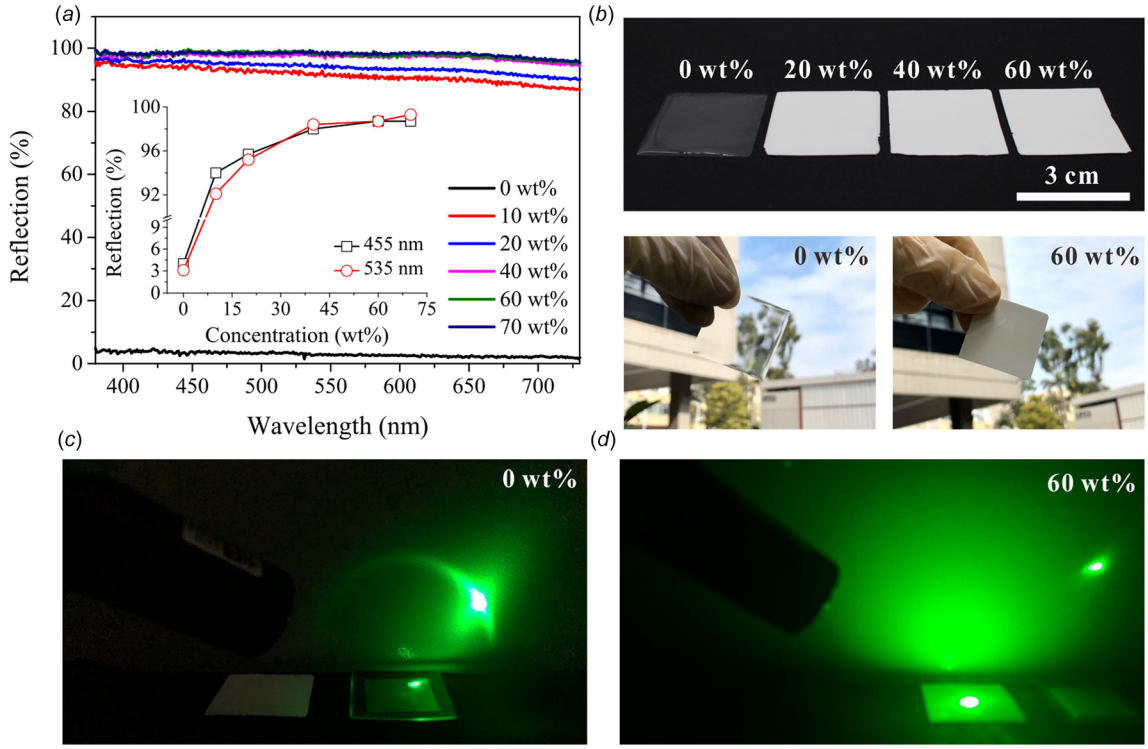

Fig. 7 (*a*) Reflection spectra of BNR with different BN concentrations. The thickness is 400 μm. The insert gives the concentration-dependent reflection for typical wavelengths of 455 and 535 nm, respectively. (*b*) Photographs of BNR with different BN concentration under daylight. (*c*) Photographs of BNR under sunlight to show the transmittance. (*d*) Photographs of BNR under green laser to show the diffusion reflection.

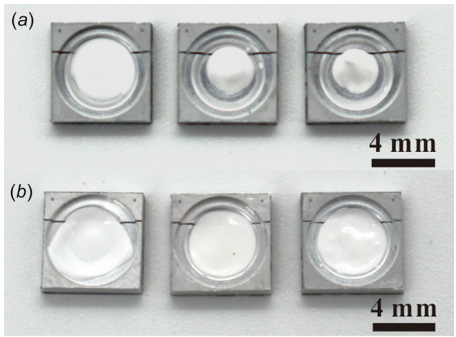

Fig. 8 Photographs of BNR coating on the lead frame with different BN concentration. (*a*) Casting BNR without centrifugation. (*b*) BNR with centrifugation. The centrifugal speed and time is 4500 rpm and 75 s, respectively. The concentration is 40, 60, and 70 wt % from left to right, respectively.

is kept at 400 μm. The reflectance reaches as high as ~90% incorporating with only 10 wt % BN nanoparticles, confirming their excellent back-scattered ability for reflection enhancement. As the BN concentration increases, the reflectance keeps increasing and becomes saturated at the BN concentration over 40 wt %. The reflectance for two typical wavelengths, blue (455 nm) and green (535 nm) used in our cases, is summarized in the insert, which is as high as ~99% for both wavelengths after the BN concentration over 40 wt %. The photographs of these BNR are also given in Fig. 7(*b*), where the visible light is hardly transmitted at a high BN concentration (Fig. 7(*c*)) and exhibits a strong diffusion reflection (Fig. 7(*d*)).

From the prospective of optical efficiency, the BN concentration over 40 wt % (at the case of 400 μm) is satisfied owing to its high reflectance. Actually, the BN concentration should be as high as possible, considering the thermal conductivity of BNR for effective heat dissipation. However, there is a tradeoff that it is difficulty to casting the BNR in the lead frame owing to the strong viscous force at a high BN concentration. As shown in Fig. 8(*a*), the casting BNR appears irregular shape and is not entirely covered in the lead frame even though with a low BN concentration of 40 wt %. Therefore, we have introduced the centrifugal process with good repeatability and consistency to overcome this limitation. As shown in Fig. 8(*b*), the BNR with a high BN concentration is regularly and entirely covered in the lead frame after centrifugation at a speed of 4500 rpm for 75 s. However, the BNR with 70 wt % concentration is hardly coated with a regular shape owing to the insufficient centrifugal force in our cases. As a result, BN concentration of 60 wt % is selected for subsequent investigations.

The equilibrium geometry of BNR can be determined by the gravity, surface tension, and the centrifugal force by minimizing the total free energy [39,40]. Herein, the centrifugal force is used to adjust the equilibrium geometry of BNR by changing the centrifugal speed, as shown in Fig. 9(*a*). A convex BNR structure is observed at a low centrifugal speed, demonstrating that the centrifugal force is not large enough to overcome the surface tension of the BNR. As the centrifugal speed increases, the planar and concave structures are observed in sequence. It is worth to mention that a portion of BN composites is easily sputtered out of the lead frame when the centrifugal speed is higher than 4500 rpm, which is out of the consideration in our cases. The radiant power of inverted BNR-LEDs with different centrifugal speed is given in Fig. 9(*b*), which increases as the centrifugal speed increases. The inverted BNR-LEDs using 4500 rpm have a radiant power of 22.3% larger than that using 3000 rpm, demonstrating that the geometry of BNR is critical for achieving high optical efficiency. As discussed above, a convex shape is obtained at a low centrifugal speed of 3000 rpm; most of blue light from chips reaching at the BNR surface with small incident angles has been reflected toward large emission angles as shown in Fig. 9(*c*). As a result, a portion of reflected blue light propagates into the ITO glass with large incident angles, suffering from serious Fresnel flection loss; while a portion of reflected blue light directly propagates into the lead frame, causing much absorption loss. As the centrifugal speed increases to 3500 rpm, an approximately planar geometry is obtained. Compared with the convex BNR structure, the reflection angles of blue light can be treated as the same as the incident angles in the planar BNR structure as shown in Fig. 9(*d*). This means that the reflection angles of blue light are without expansion, which easily propagates into the ITO glass keeping their

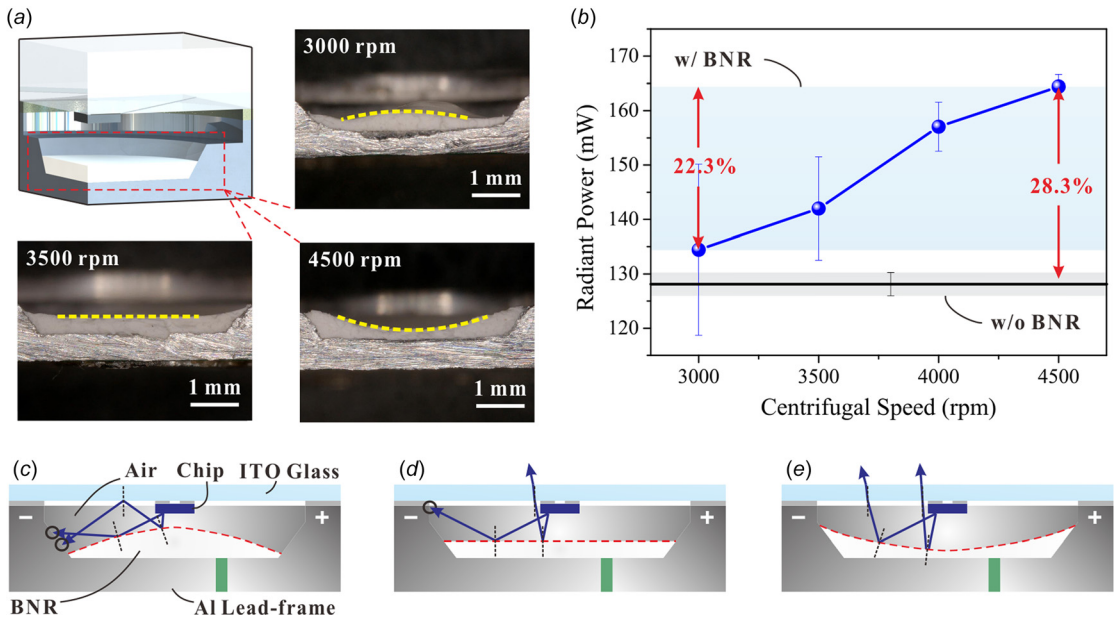

Fig. 9 Optical efficiency of inverted BNR-LEDs with different centrifugal speed. (*a*) Photographs of inverted BNR-LEDs with different centrifugal speed. The diagram at the top-left is the cross-sectional view of inverted BNR-LEDs. (*b*) Radiant power of blue inverted LEDs. ((*c*)–(*e*)) Diagrams of light-extraction mechanisms of inverted BNR-LEDs with convex, planar, and concave BNR structure, respectively.

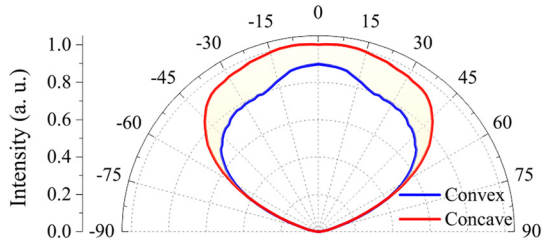

Fig. 10 Typical intensity distributions of inverted BNR-LEDs

small reflection angles and leads to less Fresnel reflection loss. As the centrifugal speed increases over 4000 rpm, the planar structure is gradually transited to the concave structure. Further compared with the planar BNR structure, the reflection angles of blue light are reduced compared with the incident angles at the concave BNR surface as shown in Fig. 9(*e*). The concave BNR structure is similar to the spotlight reflector to redirect the incident light toward small emission angles, which is beneficial for the blue light propagating into the ITO glass with smaller incident angles. To further support this explanations, the intensity distributions of concave and convex structures are given in Fig. 10. The concave structure has a larger intensity at the emission angles within ±60 degree compared with the convex structure. Especially, the intensity enhancement is much higher at large angles (from 15 to 60 degree), further confirming that the concave BNR structure is more beneficial to extract the blue light with large emission angles from the LED chip by reducing the reflection angles. *Therefore, a maximum radiant power is achieved using a concave BNR structure. Moreover, all the inverted BNR-LEDs have a higher radiant power even using the convex structure compared with conventional inverted LEDs, which is mainly attributed to the high reflectance of BNR. After geometry optimizations, the concave BRN structure contributes to a radiant power increased by 28.3% compared with the conventional one for blue devices.

3.3 Effect of Boron Nitride-Incorporating Reflector Structure on Quantum Dot Light Extraction. The optical performances of inverted QD/BNR-LEDs with different centrifugal speed are also investigated, and their electroluminescence (EL) spectra are shown in Fig. 11(*a*). The wavelengths in the blue region from 400 to 500 nm are regarded as chip light while that from 500 to 600 nm are regarded as QD light, which are originated from the LED chip and QDs, respectively. The EL intensity of chip light slightly increases with the increasing centrifugal speed, and the peak intensity is increased within 10%, which is far lower than that of blue devices. However, a larger enhancement in EL intensity of QD light occurs as the centrifugal speed increases, demonstrating that the BNR structure is helpful to increase the color-conversion probability of QD converters. The radiant power proportion (RPP) of chip light and QD light, defined as radiant power ratio of the chip light (QD light) to the total light, with different centrifugal speed is given to support this notion, as shown in Fig. 11(*b*). All of QD/BNR-LEDs appear a lower RPP of chip light and a higher RPP of QD light compared with conventional QD-LEDs, confirming much more conversion events occurring in QD/BNR-LEDs. One reasonable explanation is that the reflection ability of BNR is originated from the scattering effect of BN nanoparticles. It is unsurprising that a strong diffusion reflection occurs at the BNR surface, leading to a longer optical path of blue light in the QD converter as compared in Figs. 12(*a*) and 12(*b*). To investigate this issue, the reflection distributions of BNR with different concentrations are given in Fig. 12(*c*), and a stronger diffusion reflection intensity can be observed at emission angles out of the specular angles with the increasing BN concentration.

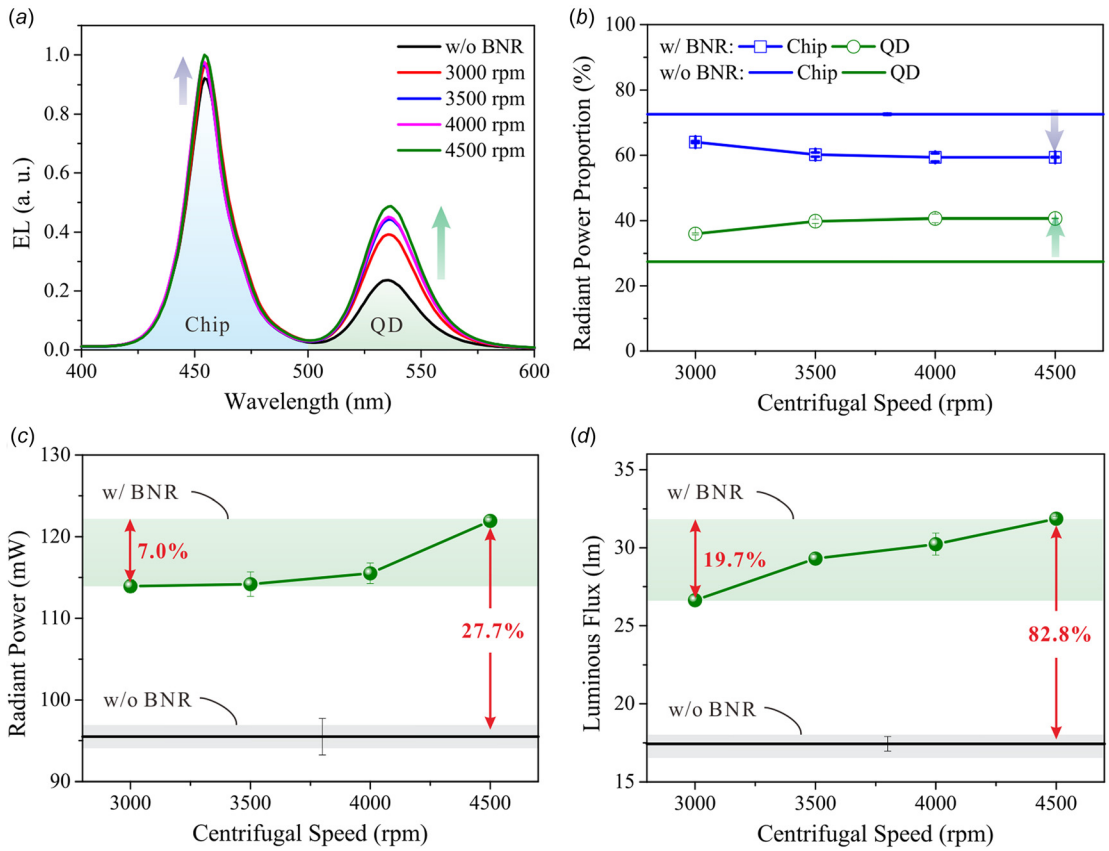

Fig. 11 Optical efficiency of inverted QD/BNR-LEDs with different centrifugal speed. (*a*) EL spectra. (*b*) Radiant power proportion of light originated from chip and QD, respectively. (*c*) Radiant power. (*d*) Luminous flux.

Furthermore, the same QD converter is assembled to each BNR with different BN concentrations, respectively. Their photoluminescence (PL) spectra are given in Fig. 12(*d*), and the 365 nm excitation light is incident from the QD side to obtain the reflected conversion light. It is obvious that the PL intensity largely increases with the increasing BN concentration, which can be confirmed by the photographs shown in Figs. 12(*e*) and 12(*f*). Moreover, the PL enhancement is summarized in the insert of Fig. 12(*d*) by integrating the corresponding PL spectra. Notably, the PL enhancement of BNR with 60 wt % concentration is further higher than that with 40 wt % concentration even though their reflectance is very similar (Fig. 6), achieving a maximum PL enhancement of 5.24 fold compared with the bare QD converter. These results suggest that the diffusion reflection of BNR largely contributes to enhancing the PL intensity of QD converters, which can well explain the enhanced EL intensity of QD light in devices after using BNR structures.

Although the dispensing mass of QD converters is the same for all structures, the RPP of QD light keeps increasing as the centrifugal speed increases as shown in Fig. 11(*b*). These results demonstrate that the geometry of QD/BNR also affects the conversion probability of QD converters. Accordingly, the cross-sectional views of QD/BNR on the lead frame with different centrifugal speed are given in Figs. 13(*a*)–13(*c*). The QD converters keep approximately planar surface determined by the low viscosity of PDMS matrix. However, they become thicker in the centered region as the centrifugal speed increases, which is influenced by their below BNR structures. This means that the blue light has a longer optical path in the centered region of QD converters as the centrifugal speed increases, as shown in Figs. 13(*d*) and 13(*e*). Moreover, the blue light in the centered region with small emission angles from chips is generally with large intensity owing to the Lambertian lighting of LEDs. This portion of blue light much more contributes to increasing the conversion events compared with that in the edge region with large emission angles from chips. As a result, the concave BNR structure is more beneficial to increase the color-conversion probability of QD converters. The radiant power of inverted QD/BNR-LEDs with different centrifugal speed is given in Fig. 11(*c*). It is interesting that the convex BNR structure (3000 rpm) also largely contributes to an enhancement by 20.7% after considering color conversion; such enhancement is far higher than that in blue devices. These results are because that much of chip light is converted to QD light before reaching the surface of BNR; the extraction of QD light is less affected by the BNR structure owing to its isotropic emission and is mainly improved by the enhanced reflection ability. As discussed above, there are much more conversion events with the increasing centrifugal speed owing to the increased optical path of chip light in the centered region of QD converters. Generally, much more conversion events are associated with a larger conversion loss. Therefore, the enhancement caused by different BNR structures in QD devices become less obvious compared with that in blue devices; the radiant power of concave BNR structure (4500 rpm) is only 7% higher than that of the convex (3000 rpm). However, a maximum increase of 27.7% is still achieved when using a concave BNR structure (4500 rpm) just similar to that in blue devices. In addition, much more conversion loss demonstrates a larger thermal power generated in the QD layer, which is not beneficial to increase the device stability. In future, there is still great improvement space for thermal performances by further

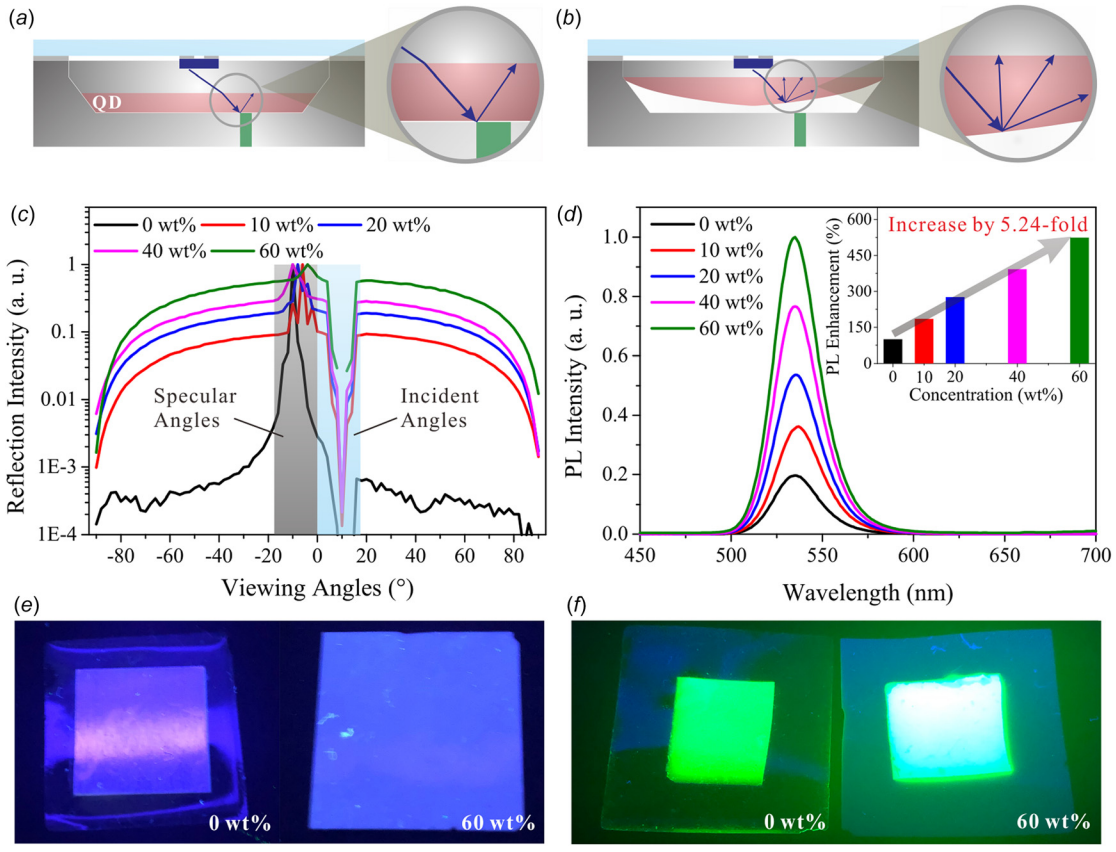

Fig. 12 Diagrams of light propagating into QD/BNR in inverted LEDs. ((*a*) and (*b*)) Diagrams of light reflection at the QD/substrate interface and the QD/BNR interface, respectively. ((*c*)) Reflection distributions of BNR with different concentration. The blue laser is used as the light source with incident angle of ~10 deg. (*d*) PL spectra of QD/BNR hybrid membranes with different BN concentrations. ((*e*) and (*f*)) BNR membranes and QD/BNR hybrid membranes under ultraviolet light with different BN concentrations. The substrate under the membrane is the polished aluminum sheet.

optimizing the structures of QD and BNR layers. The luminous flux of these devices is also given in Fig. 11(*d*), which shows a similar tendency as the radiant power. It is worth to mention that the optimized concave BNR structure (4500 rpm) contributes to a maximum increase of 82.8% compared with the reference device, which is attributed to the synergistic effect of BNR structures for enhancing light extraction and PL intensity. Therefore, we can safely indicate that the concave BNR structure is significant to increase the optical efficiency of inverted LEDs.

To provide a more comprehensive understanding of the BNR structure, the optical performance of inverted LEDs with different BNR dispensing mass is also investigated. The radiant power of blue inverted BNR-LEDs is given in Fig. 14(*a*), and the centrifugal speed is kept at 4500 rpm. The BNR dispensing mass of 1, 3, and 5 mg is corresponding to the thickness of 80, 250, and 400 μm, respectively, at the centered point. It is unsurprising that the radiant power decreases as the dispensing mass reduces probably owing to the change in geometry or reflectance, while BNR structures, even with 1 mg dispensing mass, still contribute to a larger radiant power compared with the reference. To accurately figure out the behind reason of these results, the reflectance spectra of BNR with different thickness are shown in Fig. 14(*b*); each thickness approximately corresponds to the dispensing mass of BNR in devices as illustrated above. The reflectance of BNR with the thickness between 250 and 400 μm is similar while obviously larger than that with the thickness of 80 μm. The reflectance of BNR is summarized in the insert with two typical wavelengths for convenience. These results can well explain that the radiant power reduction with decreased dispensing mass is significantly influenced by the geometry of BNR as the reflectance difference between 250 and 400 μm can be neglected. It is obvious that the curvature reduces in the thinner BNR and tends to be a planar surface. Therefore, a thicker BNR is an alternative to obtain a more concave structure to achieve a higher optical efficiency. Furthermore, QD converters are coated onto BNR to gain the inverted QD/BNR-LEDs, and their radiant power and luminous flux are given in Fig. 14(*c*). Similarly, both of their radiant power and luminous flux decrease as the dispensing mass reduces, which are still larger than that of the reference without BNR structure. In addition, their EL spectra are given in Fig. 14(*d*) to investigate this issue. It is obvious that the reduced optical efficiency can be mainly attributed to the declining EL intensity of QD light. Moreover, a slight reduction in EL intensity of QD light is still observed when the dispensing mass decreases from 5 to 3 mg although these BNR have similar reflectance spectra. The RPP of QD light is calculated and given in the insert, and a reduced RPP of QD light is also observed, demonstrating that there is a lower conversion probability as the dispensing mass reduces. As discussed in Fig. 13, these results are because that the extraction of QD light is significantly affected by the diffuse reflectance, which can be further supported by the PL spectra with different BNR thicknesses as shown in Fig. 15. An increased PL intensity is observed as the thickness increases from 250 μm to 400 μm although these BNR are with similar reflectance.

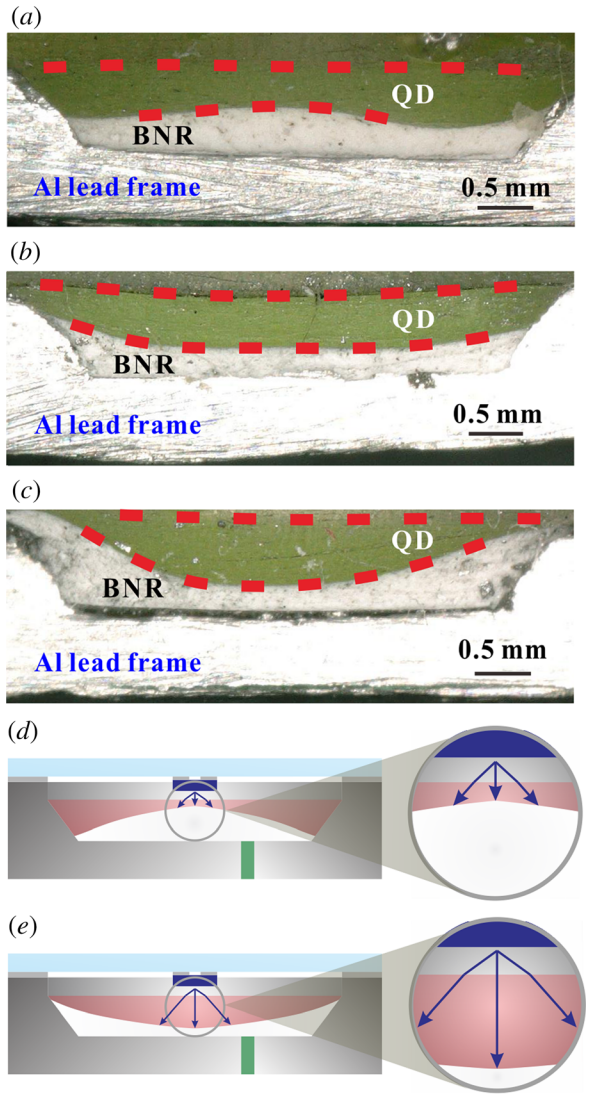

Fig. 13 ((*a*) and (*c*)) Photographs of cross-sectional views of inverted QD/BNR LEDs with centrifugal speed of 3000, 3500, and 4500 rpm, respectively. ((*d*) and (*e*)) Diagrams of blue light path in QD converters of inverted LEDs when using concave and convex BNR structure, respectively.

4 Conclusion

In this paper, we develop the scattering nanoparticles-induced reflection effect to enhance the optical efficiency of inverted QD-LEDs combined with a centrifugation technique. The scattering effect of nanoparticles on the reflection performance of inverted LEDs is investigated using the ray-tracing and FDTD methods. Results indicate that a stronger back-scattered ability of nanoparticles is beneficial to increase the reflection performance when compared at the same scattering coefficient. Moreover, the back-scattered ability of two typical structures of nanoparticles (spherical and columnar structures) is investigated, demonstrating that the thin columnar structures are highly expected to enhance the back-scattered energy proportion. These results are mainly attributed to the Rayleigh scattering for light perpendicularly incident into the end surface of the thin columnar nanoparticle. Therefore, a solid guideline is provided to choose the BN nanoparticles with a thin columnar structure as scattered centers in the reflection layer of inverted QD-LEDs. Herein, a centrifugation technique is introduced to achieve the equilibrium geometry for BNR structures by balancing their viscosity (surface tension). The centrifugal speed is used to control the equilibrium geometry of BNR structures, indicating that the concave BNR structure with the light concentrating effect is most beneficial to increase the optical efficiency for blue light, which can be attributed to the less Fresnel reflection loss of reflected blue light at the surface of the ITO glass. After coating with QD layers, the optimized concave BNR structure further increases the color-conversion probability and boosts an increase of 82.8% in luminous flux compared with the conventional inverted QD-LEDs, which is simultaneously resulted from the light concentrated effect of the concave geometry and the strong diffusion reflection ability of BN nanoparticles. Consequently, the concave reflection layer incorporated with thin columnar BN nanoparticles plays a significant role in enhancing the optical efficiency of inverted LEDs.

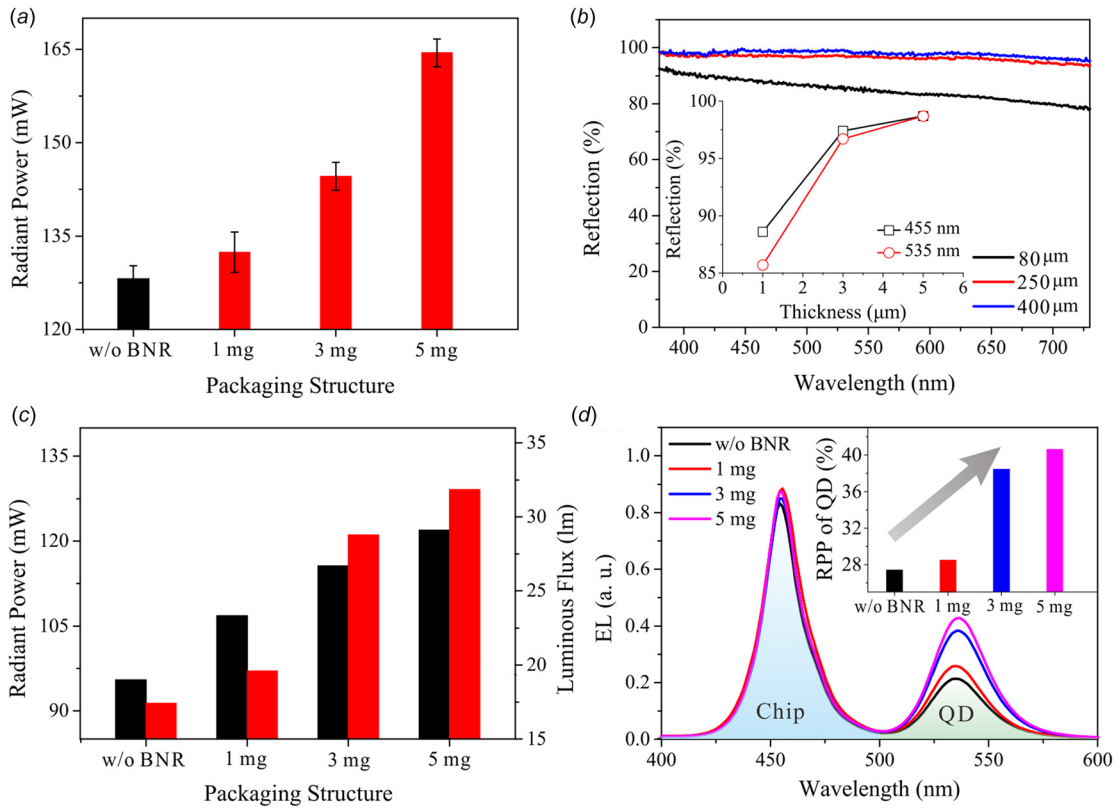

Fig. 14 Optical efficiency of inverted QD/BNR-LEDs with different BNR dispensing mass. (*a*) Radiant power of inverted BNR-LEDs. The insert shows their intensity distribution. (*b*) Reflection spectra of BNR with different thickness and a constant BN concentration of 60 wt %. The insert gives the thickness-dependent reflection for typical wavelengths of 455 and 535 nm, respectively. (*c*) Radiant power and luminous flux of inverted QD/BNR-LEDs. (*d*) EL spectra of inverted QD/BNR-LEDs. The insert shows the RPP of QD light when using different BNR dispensing mass.

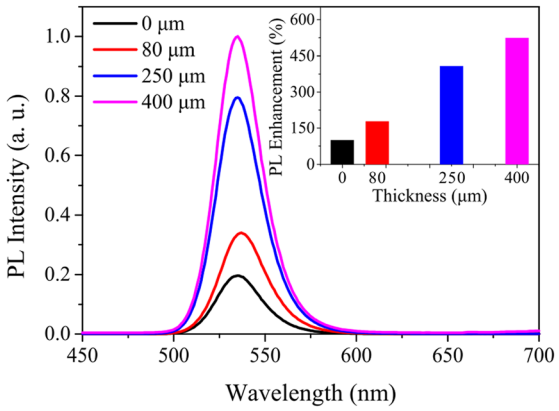

Fig. 15 Photoluminescence spectra of QD/BNR hybrid membranes with different BNR thicknesses

In future, we plan to optimize the QD/BNR hybrid structures to comprehensively improve the optical and thermal performances for inverted LEDs.

Funding Data

- National Natural Science Foundation of China (Nos. 51735004 and 51775199; Funder ID: 10.13039/501100001809).
- Project of Science and Technology New Star in Zhujiang Guangzhou City (No. 201806010102; Funder ID: 10.13039/501100004000).
- Natural Science Foundation of Guangdong Province (No. 2014A030312017; Funder ID: 10.13039/501100003453).

References

[1] Pust, P., Schmidt, P. J., and Schnick, W., 2015, "A Revolution in Lighting," Nat. Mater., **14**(5), pp. 454–458.

[2] Nakamura, S., Mukai, T., and Senoh, M., 1994, "Candela-Class High-Brightness InGaN/AlGaN Double-Heterostructure Blue-Light-Emitting Diodes," Appl. Phys. Lett., **64**(13), pp. 1687–1689.

[3] Jang, E., Jun, S., Jang, H., Lim, J., Kim, B., and Kim, Y., 2010, "White-Light-Emitting Diodes With Quantum Dot Color Converters for Display Backlights," Adv. Mater., **22**(28), pp. 3076–3080.

[4] Li, Z. T., Cao, K., Li, J. S., Tang, Y., Xu, L., Ding, X. R., and Yu, B. H., 2019, "Investigation of Light-Extraction Mechanisms of Multiscale Patterned Arrays With Rough Morphology for GaN-Based Thin-Film LEDs," IEEE Access, **7**, pp. 73890–73898.

[5] Ye, S., Xiao, F., Pan, Y., Ma, Y., and Zhang, Q., 2010, "Phosphors in Phosphor-Converted White Light-Emitting Diodes: Recent Advances in Materials, Techniques and Properties," Mater. Sci. Eng. R: Rep., **71**(1), pp. 1–34.

[6] Chen, K.-J., Chen, H.-C., Shih, M.-H., Wang, C.-H., Tsai, H.-H., Chien, S.-H., Lin, C. C., and Kuo, H.-C., 2013, "Enhanced Luminous Efficiency of WLEDs Using a Dual-Layer Structure of the Remote Phosphor Package," J. Lightwave Technol., **31**, pp. 1941–1945.

[7] Tsai, P.-Y., Huang, H.-K., Sung, J.-M., Kan, M.-C., and Wang, Y.-H., 2015, "High Thermal Stability and Wide Angle of White Light Chip-on-Board Package Using a Remote Phosphor Structure," IEEE Electron Device Lett., **36**(3), pp. 250–252.

[8] Li, Z., Yong, T., Li, J., Wu, C., Ding, X., and Yu, B., 2018, "High Color Uniformity of White Light-Emitting Diodes Using Chip-Scaled Package," IEEE Photonics Technol. Lett., **30**(11), pp. 989–992.

[9] Li, Z., Song, C., Li, J., Liang, G., Rao, L., Yu, S., Ding, X., Tang, Y., Yu, B., Ou, J., Lemmer, U., and Gomard, G., 2020, "Highly Efficient and Water-Stable Lead Halide Perovskite Quantum Dots Using Superhydrophobic Aerogel Inorganic Matrix for White Light-Emitting Diodes," Adv. Mater. Technol., **5**(2), p. 1900941.

[10] Huang Chen, S.-W., Shen, C.-C., Wu, T., Liao, Z.-Y., Chen, L.-F., Zhou, J.-R., Lee, C.-F., Lin, C.-H., Lin, C.-C., Sher, C.-W., Lee, P.-T., Tzou, A.-J., Chen,

Z., and Kuo, H.-C., 2019, "Full-Color Monolithic Hybrid Quantum Dot Nanoring Micro Light-Emitting Diodes With Improved Efficiency Using Atomic Layer Deposition and Nonradiative Resonant Energy Transfer," Photonics Res., **7**(4), pp. 416–422.
[11] Xie, B., Liu, H., Hu, R., Wang, C., Hao, J., Wang, K., and Luo, X., 2018, "Targeting Cooling for Quantum Dots in White QDs-LEDs by Hexagonal Boron Nitride Platelets With Electrostatic Bonding," Adv. Funct. Mater., **28**(30), p. 1801407.
[12] Li, J., Tang, Y., Li, Z., Ding, X., Yu, B., and Lin, L., 2019, "Largely Enhancing Luminous Efficacy, Color-Conversion Efficiency, and Stability for Quantum Dot White LEDs Using the Two-Dimensional Hexagonal Pore Structure of SBA-15 Mesoporous Particles," ACS Appl. Mater. Interfaces, **11**(20), pp. 18808–18816.
[13] Chen, H. W., Zhu, R. D., He, J., Duan, W., Hu, W., Lu, Y. Q., Li, M. C., Lee, S. L., Dong, Y. J., and Wu, S. T., 2017, "Going Beyond the Limit of an LCD's Color Gamut," Light Sci. Appl., **6**(9), p. e17043.
[14] Wu, T., Sher, C.-W., Lin, Y., Lee, C.-F., Liang, S., Lu, Y., Huang Chen, S.-W., Guo, W., Kuo, H.-C., and Chen, Z., 2018, "Mini-LED and Micro-LED: Promising Candidates for the Next Generation Display Technology," Appl. Sci., **8**(9), p. 1557.
[15] Kim, T.-H., Jun, S., Cho, K.-S., Choi, B. L., and Jang, E., 2013, "Bright and Stable Quantum Dots and Their Applications in Full-Color Displays," MRS Bull., **38**(9), pp. 712–720.
[16] Han, H.-V., Lin, H.-Y., Lin, C.-C., Chong, W.-C., Li, J.-R., Chen, K.-J., Yu, P., Chen, T.-M., Chen, H.-M., Lau, K.-M., and Kuo, H.-C., 2015, "Resonant-Enhanced Full-Color Emission of Quantum-Dot-Based Micro LED Display Technology," Opt. Express, **23**(25), pp. 32504–32515.
[17] Lin, H.-Y., Sher, C.-W., Hsieh, D.-H., Chen, X.-Y., Chen, H.-M. P., Chen, T.-M., Lau, K.-M., Chen, C.-H., Lin, C.-C., and Kuo, H.-C., 2017, "Optical Cross-Talk Reduction in a Quantum-Dot-Based Full-Color Micro-Light-Emitting-Diode Display by a Lithographic-Fabricated Photoresist Mold," Photonics Res., **5**(5), pp. 411–416.
[18] Li, J. S., Tang, Y., Li, Z. T., Ding, X. R., Rao, L. S., and Yu, B. H., 2018, "Effect of Quantum Dot Scattering and Absorption on the Optical Performance of White Light-Emitting Diodes," IEEE Trans. Electron Devices, **65**(7), pp. 2877–2884.
[19] Sher, C.-W., Lin, C.-H., Lin, H.-Y., Lin, C.-C., Huang, C.-H., Chen, K.-J., Li, J.-R., Wang, K.-Y., Tu, H.-H., Fu, C.-C., and Kuo, H.-C., 2016, "High Quality Liquid-Type Quantum Dots White Light-Emitting Diode," Nanoscale, **8**(2), pp. 1117–1122.
[20] Li, J.-S., Tang, Y., Li, Z.-T., Rao, L.-S., Ding, X.-R., and Yu, B.-H., 2018, "High Efficiency Solid–Liquid Hybrid-State Quantum Dot Light-Emitting Diodes," Photonics Res., **6**(12), pp. 1107–1115.
[21] Sadeghi, S., Kumar, B. G., Melikov, R., Aria, M. M., Jalali, H. B., and Nizamoglu, S., 2018, "Quantum Dot White LEDs With High Luminous Efficiency," Optica, **5**(7), pp. 793–802.
[22] Li, J., Tang, Y., Li, Z., Ding, X., Rao, L., and Yu, B., 2019, "Investigation of Stability and Optical Performance of Quantum-Dot-Based LEDs With Methyl-terminated-PDMS-Based Liquid-Type Packaging Structure," Opt. Lett., **44**(1), pp. 90–93.
[23] Wang, H., Mou, Y., Peng, Y., Liu, J., Liang, R., Chen, M., Dai, J., and Chen, C., 2019, "White Light-Emitting Diodes With High Color Quality Fabricated Using Phosphor-in-Glass Integrated With Liquid-Type Quantum Dot," IEEE Electron Device Lett., **40**(4), pp. 601–604.
[24] Li, J.-S., Tang, Y., Li, Z.-T., Kang, W.-Q., Ding, X.-R., and Yu, B.-H., 2019, "Study on Reabsorption Properties of Quantum Dot Color Convertors for Light-Emitting Diode Packaging," ASME J. Electron. Packag., **141**(4), p. 041006.
[25] Xie, B., Liu, H., Sun, X., Yu, X., Wu, R., Wang, K., and Luo, X., 2019, "Reduced Working Temperature of Quantum Dots-Light-Emitting Diodes Optimized by Quantum Dots at Silica-on-Chip Structure," ASME J. Electron. Packag., **141**(3), p. 031001.
[26] Li, J.-S., Tang, Y., Li, Z.-T., Liang, G.-W., Ding, X.-R., and Yu, B.-H., 2019, "High Thermal Performance and Reliability of Quantum-Dot-Based Light-Emitting Diodes With Watt-Level Injection Power," IEEE Trans. Device Mater. Reliab., **19**(1), pp. 120–125.
[27] Li, Z. T., Li, J. X., Li, J. S., Du, X. W., Song, C. J., and Tang, Y., 2019, "Thermal Impact of LED Chips on Quantum Dots in Remote-Chip and on-Chip Packaging Structures," IEEE Trans. Electron Devices, **66**(11), pp. 4817–4822.
[28] Woo, J. Y., Kim, K. N., Jeong, S., and Han, C.-S., 2010, "Thermal Behavior of a Quantum Dot Nanocomposite as a Color Converting Material and Its Application to White LED," Nanotechnology, **21**(49), p. 495704.
[29] Abe, S., Joos, J. J., Martin, L. I., Hens, Z., and Smet, P. F., 2017, "Hybrid Remote Quantum Dot/Powder Phosphor Designs for Display Backlights," Light: Sci. Appl., **6**(6), p. e16271.
[30] Tang, Y., Lu, H. G., Li, J. S., Li, Z. T., Du, X. W., Ding, X. R., and Yu, B. H., 2019, "Improvement of Optical and Thermal Properties for Quantum Dots WLEDs by Controlling Layer Location," IEEE Access, **7**, pp. 77642–77648.
[31] Xie, B., Chen, W., Hao, J., Wu, D., Yu, X., Chen, Y., Hu, R., Wang, K., and Luo, X., 2016, "Structural Optimization for Remote White Light-Emitting Diodes With Quantum Dots and Phosphor: Packaging Sequence Matters," Opt. Express, **24**(26), pp. A1560–A1570.
[32] Lei, X., Zheng, H., Guo, X., Chu, J., Liu, S., and Liu, P., 2016, "Optical Performance Enhancement of Quantum Dot-Based Light-Emitting Diodes Through an Optimized Remote Structure," IEEE Trans. Electron Devices, **63**(2), pp. 691–697.
[33] Li, Z. T., Song, C. J., Qiu, Z. Y., Li, J. S., Cao, K., Ding, X. R., and Tang, Y., 2019, "Study on the Thermal and Optical Performance of Quantum Dot White Light-Emitting Diodes Using Metal-Based Inverted Packaging Structure," IEEE Trans. Electron Devices, **66**(7), pp. 3020–3027.
[34] Chen, K.-J., Han, H.-V., Chen, H.-C., Lin, C.-C., Chien, S.-H., Huang, C.-C., Chen, T.-M., Shih, M.-H., and Kuo, H.-C., 2014, "White Light Emitting Diodes With Enhanced CCT Uniformity and Luminous Flux Using ZrO_2 Nanoparticles," Nanoscale, **6**(10), pp. 5378–5383.
[35] Tang, Y., Li, Z., Li, Z. T., Li, J. S., Yu, S. D., and Rao, L. S., 2018, "Enhancement of Luminous Efficiency and Uniformity of CCT for Quantum Dot-Converted LEDs by Incorporating With ZnO Nanoparticles," IEEE Trans. Electron Devices, **65**(1), pp. 158–164.
[36] Flock, S. T., Patterson, M. S., Wilson, B. C., and Wyman, D. R., 1989, "Monte Carlo Modeling of Light Propagation in Highly Scattering Tissues. I. Model Predictions and Comparison With Diffusion Theory," IEEE Trans. Biomed. Eng., **36**(12), pp. 1162–1168.
[37] Jones, A., 1999, "Light Scattering for Particle Characterization," Prog. Energy Combust. Sci., **25**(1), pp. 1–53.
[38] Li, J., Chen, J., Lin, L., Li, Z., Tang, Y., Yu, B., and Ding, X., 2015, "A Detailed Study on Phosphor-Converted Light-Emitting Diodes With Multi-Phosphor Configuration Using the Finite Difference Time-Domain and Ray-Tracing Methods," IEEE J. Quantum Electron., **51**(10), pp. 1–10.
[39] Brakke, K. A., 1992, "The Surface Evolver," Exp. Math., **1**(2), pp. 141–165.
[40] Chou, T.-H., Hong, S.-J., Liang, Y.-E., Tsao, H.-K., and Sheng, Y.-J., 2011, "Equilibrium Phase Diagram of Drop-on-Fiber: Coexistent States and Gravity Effect," Langmuir, **27**(7), pp. 3685–3692.